DIFFRACTION OF SOUND WAVES BY A PERIODIC FAÇADE DISPLAYING IMPEDANCE BOUNDARY CONDITIONS

François-Marie Lucchetti[1], Stéphane Ancey[1], Paul Gabrielli[1], Michaël Mercier[1]
[1] *UMR CNRS 6134 SPE, Université de Corse, France*

This paper is a revised version of the authors' submitted manuscript that was peer-reviewed by at least two anonymous reviewers.

Abstract

Our study aims to develop an analytical and numerical model to quantify the influence of a building's façade geometry and all its components (windows, balconies, etc.) on scattered and reflected sound waves. We have therefore chosen to adapt a diffraction model originally used in underwater acoustics and elastodynamics for ultrasonic waves and to apply it to airborne acoustics for a frequency range corresponding to urban noise. This formalism, based on the expansion of the potential solutions of the Helmholtz equation into infinite series of plane waves, allows calculating the intensity maxima of far-field diffraction lobes when the studied grating is periodic. Impedance boundary conditions are applied to the surface to take account of the physical properties of the building materials used in the façade. We also provide finite element simulations and compare our model with experimental measurements taken on a 1:20 scale model under the same assumptions for a Galois diffraction grating (GF(2^3)). This profile, derived from number theory and widely used in room acoustics, attenuates the intensity of the specular lobe at a characteristic frequency. Numerical results are compared with experimental data and finite element simulations, showing good agreement and demonstrating the model's ability to predict diffraction patterns for building façades.

Keywords: *acoustic scattering, urban noise, building renovation, diffraction gratings.*

1. Introduction

Noise, whether at the scale of a street or a building, is a major public health issue. One of the keys to addressing this problem lies in considering acoustic comfort during the construction or renovation of buildings. Indeed, the geometry of façades, as well as the materials that compose them, plays an essential role in the reflection of acoustic waves within a street and their transmission into buildings. The impact of different façade elements (windows, balconies, guardrails, sunshades and so on) on sound scattering into streets has been widely studied in the literature [1], [2], [3]. Similarly, the acoustic behavior of conventional materials (those already used in buildings), as well as innovative materials (such as bio-sourced, geo-sourced, or recycled-content materials), has been the subject of numerous publications [4], [5], [6]. Finally, more theoretical work has also been conducted on the diffusion of waves by different surface profiles, including diffraction gratings [7], [8], [9].

This article extends the work initiated by Lucchetti and al. [10] on the impact of building façade geometry on the reflection and scattering of acoustic waves, taking into account the physical characteristics of the materials. This study involves adapting to the context of airborne acoustics a diffraction model, initially developed by Tamir and Bertoni [11], extended by Claeys and al. [12] and Gabrielli [13]. The resulting model uses the expansion of the potential solutions of the Helmholtz equation into infinite series of plane waves, for which distinct impedance conditions are applied to the façade under study. This method is based on a diffraction model. It is particularly well suited to our study, namely its application to low frequencies for cavity dimensions comparable to the typical dimensions of building façade elements. The results from our model are compared, on the one hand, with those obtained from a finite element code and, on the other hand, with experimental measurements on a 1:20 scale model. The studied surface is a Galois diffraction grating derived from the GF(2^3) field sequence, which reduces the specular lobe intensity at a chosen characteristic frequency. This property has been applied in room acoustics particularly in theaters and museums [14]. Schroeder [15] and Berkhout [16] further highlighted the angular distribution of intensity scattered by this profile at the characteristic frequency.

Corresponding author: *lucchetti_f@univ-corse.fr.*

2. Problem statement

As part of our study, we chose to use a periodic diffraction grating of type GF(2^3) (see Figure 1). This geometry has the advantage of providing maximum attenuation of the reflected intensity in the specular direction at its characteristic frequency f_0, due to the mechanism of destructive wave interference. We denote by λ_0 the wavelength associated with this frequency. We define the "front faces" as the positions of the surface profile at $z = 0$, the "cavity bottoms" as those at the depth $z = \frac{\lambda_0}{4}$ and the "cavity edges" as the separation between them.

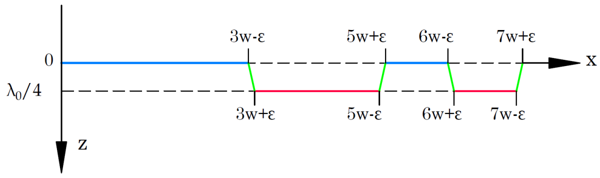

Figure 1: Surface profile of a single period Λ based on a one-dimensional Galois Field GF(2^3).

The numerical values and results presented below are based on the 1:20 scale model study. The chosen depth along the z-axis is equal to $\frac{\lambda_0}{4} = 18\,\mathrm{mm}$ which sets the characteristic frequency to $f_0 = 4790\,\mathrm{Hz}$. Each period Λ of the grating is composed of 7 elementary units of width $w = \frac{\lambda_0}{2} = 36\,\mathrm{mm}$. The cavity edges are defined using a slope that depends on ε in order to obtain a continuous function describing the surface profile, thereby allowing the implementation of different boundary conditions on these parts. We then let ε tend to 0 in order to approach the real case where these parts are perpendicular to the façade. It should be noted that, at the full scale, the corresponding depth is 36 cm, the characteristic frequency $f_0 = 239.5\,\mathrm{Hz}$, the width of the elementary unit 72 cm and the total length of the façade 21.24 m. These values are consistent with the typical dimensions of a building façade.

3. Wave scattering by a periodic grating

3.1. Mathematical formalism

The fluid–solid interface is defined by

$$\phi_{1,2}(x, z) = f(x) - z. \tag{1}$$

The function $f(x)$ represents the surface profile of the grating in the (x, z) plane, where x denotes the horizontal coordinate along the façade and z denotes the vertical coordinate (depth) perpendicular to the façade surface. The function $f(x)$ describes the height variation of the surface relative to the reference plane $z = 0$, with units of meters.
The scalar potential associated with the incident plane wave is given by

$$\varphi_{inc} = e^{i(k_x x + k_z z)}, \tag{2}$$

where the time dependence $e^{-i\omega t}$ is assumed. The quantities k_x and k_z are the components of the incident wave vector.
The scalar potential associated with the reflected wave is sought in the form of an infinite series of plane waves

$$\varphi_r(x, z) = \sum_{p=-\infty}^{\infty} R_p e^{i(k_p x - K_p z)} \tag{3}$$

with

$$K_p{}^2 = \frac{\omega^2}{v^2} - k_p{}^2. \tag{4}$$

The quantities k_p and K_p are respectively the horizontal and vertical components of the p-th diffracted wave vector.
$\varphi_r(x, z)$ satisfies the Helmholtz equation

$$\frac{\partial^2 \varphi_r}{\partial x^2} + \frac{\partial^2 \varphi_r}{\partial z^2} + \frac{\omega^2}{v^2}\varphi_r = 0. \tag{5}$$

3.2. Boundary conditions

The analytical–numerical model allows any type of boundary condition to be considered. Here, we choose to implement impedance boundary conditions, which take into account the physical properties of each surface element of the grating. These conditions are expressed as

$$\overrightarrow{\mathrm{grad}}\,(\varphi_{inc} + \varphi_r) \cdot \overrightarrow{\mathrm{grad}}\,(\phi_{1,2}) + \frac{ik}{\zeta_j}(\varphi_{inc} + \varphi_r) = 0, \quad \text{on } \phi_{1,2}(x, z) = 0 \tag{6}$$

with ζ_j being the reduced specific acoustic impedance over all or part of the surface profile. Thus, we can handle the case of a uniform impedance over the entire surface profile, as well as the – more realistic – case of different impedances on the front faces ($j = 1$), edges ($j = 2$) and cavity bottoms ($j = 3$). In the latter case, the resulting equation is

$$\sum_{p=-\infty}^{\infty} R_p \sum_{j=1}^{3} \left(k_p k_m - \left(\frac{\omega}{v}\right)^2 - \frac{\omega}{v\zeta_j} K_p \right) I^{r\pm}_{mp,j} = \sum_{j=1}^{3} \left(k_x k_m - \left(\frac{\omega}{v}\right)^2 + \frac{\omega}{v\zeta_j} k_z \right) I^{0}_{m,j}. \tag{7}$$

The subscripts m and p denote the different diffraction orders. The terms $I^{r\pm}_{mp,i}$ and $I^{0}_{m,i}$ correspond to the integrals to be calculated. These depend mainly on the surface profile under study. Their expressions are given by:

$$I_{mp}^{r\pm} = \begin{cases} \dfrac{1}{K_p} \displaystyle\int_0^{\Lambda} e^{i\frac{2\pi}{\Lambda}(p-m)x} e^{\pm i K_p f(x)}\, dx \\ \qquad\qquad\qquad\qquad \text{if } K_p \neq 0 \\ \pm i \displaystyle\int_0^{\Lambda} e^{i\frac{2\pi}{\Lambda}(p-m)x} f(x)\, dx \\ \qquad\qquad\qquad\qquad \text{if } K_p = 0 \end{cases} \tag{8}$$

$$I_m^0 = \frac{1}{k_z} \int_0^{\Lambda} e^{i\frac{2\pi}{\Lambda}(N-m)x} e^{i k_z f(x)}\, dx, \tag{9}$$

where N is an integer corresponding to the value of p associated with the angle of specular reflection. It should be noted that the expressions (8) and (9) do not depend on the boundary conditions applied to the surface profile.

The expression (7) corresponds to an infinite system of algebraic equations. The resolution consists of determining the unknown coefficients R_P numerically. We solve the truncated system by replacing the infinite sum with the sum $\sum_{p=-P}^{+P}$, in order to obtain a linear matrix system that can be solved using a direct method (MATLAB® [17]). The choice of the truncation order P depends on the required degree of accuracy and the numerical stability of the matrix system. Underestimating this order compromises accuracy, while overestimating it affects stability.

4. Results

The results from our model are compared, on the one hand, with those obtained from a finite element code using the software COMSOL Multiphysics® [18] and, on the other hand, with experimental measurements. The surface profile studied consists of 4 repetitions of the basic GF(2^3) pattern. We added a front surface part composed of 3 elementary units so that the profile is closer to a real façade. The characteristic frequency is 4790 Hz. The materials used are described below:

- 18 mm thick plywood panels for the front faces and cavity edges,
- 2 mm thick synthetic glass for the cavity bottoms.

A photograph of the model is presented in Figure 2.

Figure 2: Photograph of the experimental scale model built by the University's acoustics laboratory.

Impedance measurements were carried out using BSWA® tubes [19] in a two-microphone configuration in order to characterise these materials, following the standard ISO 10534-2 method [20]. The boundary condition at the end of the tubes corresponds to a perfectly rigid and reflective surface. For each of the two materials used in the model, two samples with diameters of 100 mm (frequency ranges of 64 – 500 Hz and 250 – 1600 Hz) and 30 mm (frequency range of 1000 – 6300 Hz) were produced. The microphone spacing was set to 300 mm, 80 mm, and 22.5 mm for the low-, medium-, and high-frequency ranges, respectively. The microphones were calibrated before each series of measurements using the procedure described in the BSWA® software and the supplied calibrator. All measurements were performed at a room temperature of 21°C and relative humidity of 45%.

The impedance measurements obtained in this way were used to determine the parameters of the Champoux-Allard model [21], in particular the flow resistance value for both materials. Then, the effective impedance of the materials was determined by removing the rigid backing contribution and considering the air impedance on the rear side of the panel. This enables us to obtain noiseless values, particularly at low frequencies. We are aware that our method for estimating impedance has limitations due to the assumption of porous material used in the Champoux-Allard model ; nevertheless, the model results were successfully compared with the measured impedance. More realistic models, taking into account the interaction between the material and the air (vibrating structure), appear more appropriate and will be investigated in future work.

4.1. Comparison of the results at the characteristic frequency

In this section, we present the angular diagram obtained at the characteristic frequency of our surface profile for a plane wave at normal incidence. Figure 3 presents a comparison of the results between
(i) our analytical-numerical model,
(ii) the finite element calculation code,
(iii) a simplified model derived from the Discrete Fourier Transform (DFT) of the surface profile [15] adapted to account for the physical boundary conditions.

Our analytical and numerical model currently only allows us to determine the intensity maxima of the various diffraction lobes; this is why only the results corresponding to these directions are shown in Figure 3. As predicted by the spectral properties of Galois sequences [15], the Fourier transform of this surface profile yields a comb-like structure with $2^n - 1$ principal maxima for a Galois field of order n, as established by Schroeder [22]. The angular diagrams obtained using these three models clearly show $(2^3 - 1)$, i.e., 7 main diffraction lobes and the specular lobe exhibits an intensity attenuation of about 9 dB. We observe good agreement between our different models.

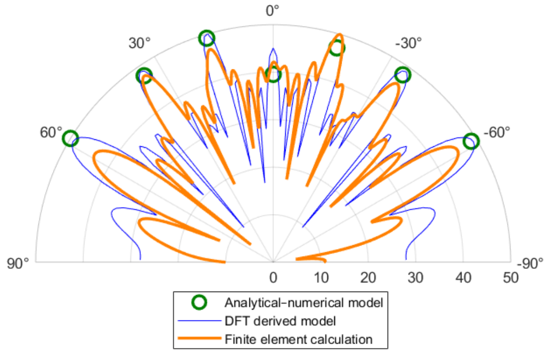

Figure 3: Angular diagrams comparison of the normalised intensity at the characteristic frequency for impedance boundary conditions.

4.2. Frequency analysis of backscattered intensity at normal incidence

4.2.1. Numerical models

We now consider the frequency dependence of the specular lobe for a plane wave under normal incidence. We investigate the frequency dependence of the diffracted sound intensity in the far field, as obtained using our analytical-numerical model. In Figure 4, we compare our results with those obtained from the finite element calculation code and the DFT derived model.

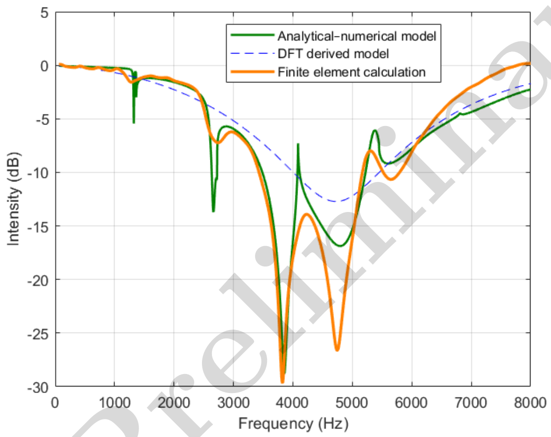

Figure 4: Frequency dependence of diffracted sound intensity in the far field for impedance boundary conditions: numerical models comparison.

A decrease in intensity is observed around the characteristic frequency ($f_0 = 4790$ Hz), which is visible on each curve. This phenomenon is consistent with theory and can be explained by the mechanism of destructive interference resulting from the difference in depth between the front faces and the bottoms of the cavities. We also observe several sudden drops in intensity around 1300 Hz, 2700 Hz, 3800 Hz and 5600 Hz, which appear in both our analytical-numerical model and our finite element code. These dips can be linked to the cut-off frequencies of the diffraction orders, at which a diffraction order becomes grazing ($\theta = \pm 90°$), leading to a redistribution of acoustic energy and an attenuation of the specular lobe. We also note a good agreement between our two models.

4.2.2. Experimental measurements

A series of measurements on the scale model was carried out in order to compare theoretical and experimental results. As there was no anechoic or semi-anechoic chamber available near our laboratory, we decided to carry out the measurements in a large hall. More specifically, we chose a sports hall with internal dimensions of 30 m × 45 m × 10.5 m. We placed our scale model in the center of the room to minimise the interference from wall reflections. We have also raised it off the ground and installed sound-absorbing materials to minimise reflections from the floor. Measurements were carried out using a Nagra Seven recorder with a 24-bit resolution and a 96 kHz sampling frequency. The data was saved in WAV format. A Sennheiser MKH 8020 microphone was used, along with a standalone unidirectional sound source, the GDB-S (01 dB). Figure 5 shows a diagram of the measurement setup. The microphone and the sound source are positioned close to one another.

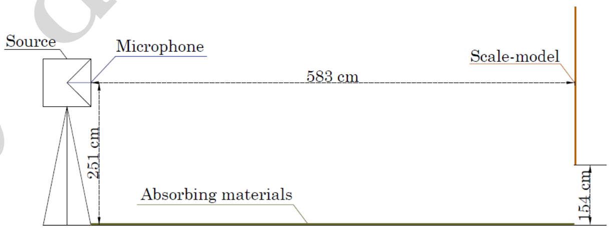

Figure 5: Schematic diagram of the experimental setup.

Scale-model measurements are generally straightforward for homogeneous objects up to a scale factor of about 20. For larger factors and longer propagation paths, however, thermal effects become significant and require compensation (e.g., by correcting for temperature and humidity variations) [23].

In order to study the acoustic reflection from the diffraction grating, the source is driven by a single period of a 4 kHz sinusoidal wave, which produces a broadband signal extending up to 8 kHz. The microphone positioned in the specular lobe in the far field records the reflected signal, capturing mainly the direct reflection. Measurements are normalised using (i) a perfectly reflective reference surface (concrete wall) or (ii) in a free-field environment by doubling the measurement distance. This latter normalisation was chosen for the results presented below in Figure 6. The normalized frequency response is obtained by subtracting the dB spectrum of the reference surface from that of the grating. This makes it possible to overcome the bandwidth limitations of the excita-

tion source, thereby allowing direct comparison of the experimental results with numerical models.
Figure 6 compares the frequency response curve of the diffracted sound intensity in the far field, as measured experimentally, with that obtained from our analytical-numerical model.

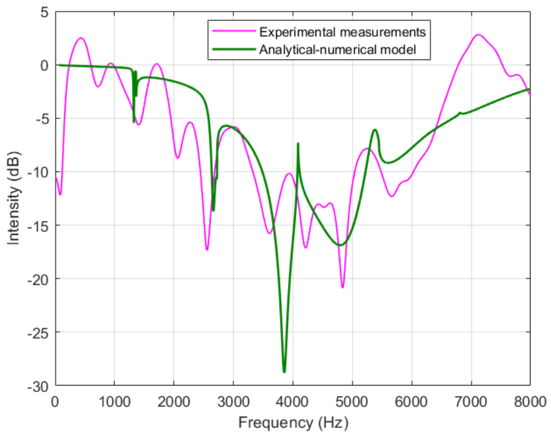

Figure 6: Frequency dependence of diffracted sound intensity in the far field for impedance boundary conditions: numerical-experimental comparison.

We notice that the decrease around the characteristic frequency ($f_0 = 4790\,\text{Hz}$) is present in both curves. This is consistent with the results already presented in Figure 4. We also observe, in relatively good agreement, the several sudden drops in intensity around 1300 Hz, 2700 Hz, 3800 Hz and 5600 Hz, which appear in both numerical and experimental curves. As mentioned previously, these dips are linked to the cut-off frequencies of the diffraction orders. The few discrepancies observed are due to the experimental conditions, and more specifically to the necessarily limited duration of the signal – a limitation required to avoid direct reflections from the ground. We are currently working on improving the experimental setup in order to minimise this effect.

5. Conclusion

We have generalised a model based on the formalism of expanding the potential solutions of the Helmholtz equation into infinite series of plane waves, in order to study the effects associated with the geometry of a building façade and the materials that compose it. The chosen surface profile is a Galois grating GF(2^3) due to its resemblance to a real building façade. The results obtained from the proposed analytical-numerical model have been compared with those derived from a finite element code, and a good agreement is observed. We also carried out a series of experimental measurements on a scale model. The initial results are promising, but the setup needs to be improved in order to minimise unwanted reflections and enhance frequency accuracy.
In the future, we plan to investigate the two-dimensional case in order to better replicate real-world conditions. We are also working on a new formulation of our model that would allow us to describe the intensity at every point in space – that is, beyond the main lobes already obtained – in order to determine the continuous angular patterns.

References

[1] E. Badino, R. Manca, L. Shtrepi, C. Calleri, and A. Astolfi, "Effect of façade shape and acoustic cladding on reduction of leisure noise levels in a street canyon," *Building and Environment*, vol. 157, pp. 242–256, Jun. 2019.

[2] P. Fausti, S. Secchi, and N. Zuccherini Martello, "The use of façade sun shading systems for the reduction of indoor and outdoor sound pressure levels," *Building Acoustics*, vol. 26, no. 3, pp. 181–206, Sep. 2019.

[3] G. M. Echevarria Sanchez, T. Van Renterghem, P. Thomas, and D. Botteldooren, "The effect of street canyon design on traffic noise exposure along roads," *Building and Environment*, vol. 97, pp. 96–110, Feb. 2016.

[4] A. D. Bella, "Comparative analysis of thermal and acoustic performance of building elements," *Forum Acusticum, Kraków, Republic of Poland*, 2014.

[5] N. Mati-Baouche et al., "Mechanical, thermal and acoustical characterizations of an insulating bio-based composite made from sunflower stalks particles and chitosan," *Industrial Crops and Products*, vol. 58, pp. 244–250, Jul. 2014.

[6] S. Schiavoni, F. DAlessandro, F. Bianchi, and F. Asdrubali, "Insulation materials for the building sector: A review and comparative analysis," *Renewable and Sustainable Energy Reviews*, vol. 62, pp. 988–1011, Sep. 2016.

[7] Hyun Ho Park and Hyo Joon Eom, "Electromagnetic scattering from multiple rectangular apertures in a thick conducting screen," *IEEE Transactions on Antennas and Propagation*, vol. 47, no. 6, pp. 1056–1060, Jun. 1999.

[8] J. F. Allard, L. Kelders, and W. Lauriks, "Ultrasonic surface waves above a doubly periodic grating," *The Journal of the Acoustical Society of America*, vol. 105, no. 4, pp. 2528–2531, Apr. 1999.

[9] A. Khanfir, "Étude des mécanismes de diffusion acoustique d'une cavité et d'un réseau à relief périodique et apériodique," Ph.D. dissertation, 2012.

[10] F.-M. Lucchetti, S. Ancey, P. Gabrielli, and M. Mercier Finidori, "Diffraction d'ondes sonores par une façade périodique présentant des conditions aux limites d'impédance," *17e Congrès Français d'Acoustique, Paris, France*, 2025.

[11] T. Tamir and H. L. Bertoni, “Lateral Displacement of Optical Beams at Multilayered and Periodic Structures,” *Journal of the Optical Society of America*, vol. 61, no. 10, pp. 1397–1413, Oct. 1971.

[12] J. M. Claeys, O. Leroy, A. Jungman, and L. Adler, “Diffraction of ultrasonic waves from periodically rough liquid–solid surface,” *Journal of Applied Physics*, vol. 54, no. 10, pp. 5657–5662, Oct. 1983.

[13] P. Gabrielli, “Diffusion d’ondes ultrasonores par des réseaux de Galois élastiques,” Ph.D. dissertation, 1995.

[14] T. Cox and P. D’Antonio, “Schroeder Diffusers: A Review,” *Building Acoustics*, vol. 10, no. 1, pp. 1–32, Mar. 2003.

[15] M. R. Schroeder, *Number theoretic phase arrays and diffraction gratings with broad radiation (Scattering) characteristics*, 1988.

[16] A. J. Berkhout, D. W. Van Wulfften Palthe, and D. De Vries, “Theory of optimal plane diffusers,” *The Journal of the Acoustical Society of America*, vol. 65, no. 5, pp. 1334–1336, May 1979.

[17] The MathWorks Inc., *Matlab version: 24.1.0.2568132 (r2024a)*, 2024. [Online]. Available: https://www.mathworks.com/

[18] COMSOL AB, *COMSOL Multiphysics®*, version 6.4, Stockholm, Sweden, 2026. [Online]. Available: https://www.comsol.com/

[19] BSWA Technology Co., Ltd., *Sw series circular impedance tube systems (sw100l / sw030l)*, https://www.bswa-tech.com/, Two-microphone transfer-function impedance tubes compliant with ISO 10534-2, ASTM E1050, and GB/T 18696.2.

[20] ISO/TC 43/SC 2, *Acoustics – determination of sound absorption coefficient and impedance in impedance tubes – part 2: Transfer-function method*, Withdrawn, Geneva, Switzerland, 1998.

[21] J.-F. Allard and Y. Champoux, “New empirical equations for sound propagation in rigid frame fibrous materials,” *The Journal of the Acoustical Society of America*, vol. 91, no. 6, pp. 3346–3353, Jun. 1992.

[22] M. R. Schroeder, “Diffuse sound reflection by maximum-length sequences,” *Journal of the Acoustical Society of America*, vol. 57, no. 1, pp. 149–150, 1975.

[23] M. R. Ismail and D. J. Oldham, “A scale model investigation of sound reflection from building façades,” *Applied Acoustics*, vol. 66, no. 2, pp. 123–147, Feb. 2005.